Supporting Information

Crystal Plane Shielding and D-Band Modulation Synergistically Achieve Durable (100) Textured Zinc Anodes

Xiangyu Ren[a], Guangwei Chen[b], Pengfei Chang[a], Shenghong Ju[b], Yunwen Wu[a*]

[a]State Key Laboratory of Metal Matrix Composites, School of Material Science and Engineering, Shanghai Jiao Tong University, Shanghai 200240, PR China

[b]China-UK Low Carbon College, Shanghai Jiao Tong University, Shanghai 201306, PR China

*Email: tlwuyunwen@sjtu.edu.cn

Experimental Section

Preparation of Electrolytes

The ZSO electrolytes were prepared by adding $ZnSO_4 \cdot 7H_2O$ (Adamas) to deionized water to prepare 2 M ZSO electrolyte as the baseline electrolyte. Various amounts of 2-butene-1,4-diol (BED) (Admas) were dissolved into 2 M ZSO electrolyte to obtain the 50mM ZSO+BED, 150mM ZSO+BED and 300mM ZSO+BED electrolytes respectively. 1,4-butanediol (BAD) and 2-butyne-1,4-diol (BYD) was added to 2 M ZSO electrolyte to obtain 150mM ZSO+BAD and ZSO+BYD.

Preparation of V_2O_5 Cathode

4.368 g commercial V_2O_5 (AR Aladdin) and 9.072 g $H_2C_2O_4$ $2H_2O$ (AR Aladdin) were dissolved in 40 mL DI water, and stirred continuously at 70 ℃ for 1 h. Then added 3 mL of the above mixed solution to 50 mL isopropanol (AR Aladdin) solution and stirred evenly. The above solution was then transferred into a Teflon-lined autoclave (100 mL) and heated at 200 ℃ for 10 h. The obtained products were filtered with water and ethanol, then blast drying at 60 ℃. Finally, the dried product was transferred to a muffle furnace and sintered at 600 ℃ for 3 h. V_2O_5 powder was obtained. V_2O_5 cathode materials were prepared by mixing V_2O_5 powder, carbon black and polyvinylidene fluoride (PVDF) with a mixing weight proportion of 7:2:1 in N-methyl-2-pyrrolidone (NMP). The obtained slurry was coated on graphite foil and the cathode materials were dried at 60 °C under a vacuum for 12 h. The V_2O_5 mass loading of the electrode was about 1-2 mg cm^{-2}.

Materials Characterizations

In situ optical microscopy (ZEISS HAL 100), laser microscopy (VK-X3000) and SEM (RISE-MAGNA) were employed to observe the morphology evolution of Zn anodes during the cycling process. XRD (Rigaku, Mini Flex 600, Cu-Kα, 40 KV, 15 mA, 5° min^{-1}) was employed to monitor the changes in crystal plane of Zn deposits under different electrolytes, and the lattice stripe spacing of the Zn deposits was analyzed by TEM (Talos F200X G2). Confocal microscopic Raman spectrometer (Renishaw in Via

Qontor, 532 nm, 28 mW) and Fourier transform infrared spectroscopy (PerkinElmer Spectrum 100) were used to characterize the electrolyte. The electron screening effect in electrolytes was investigated via nuclear magnetic resonance (NMR) spectroscopy (Bruker AVANCE III 600 MHz). *In situ* Raman was characterized by Raman spectrometer (Lab RAM Solei) and Electrochemical workstation.

Cell assembly

Zn||Zn (Zn anode with Φ=10 mm), Zn||Cu (Zn anode with Φ=10 mm, Cu electrode with Φ=10 mm) and Zn||V_2O_5 (Zn anode with Φ=16 mm, V_2O_5 cathode with Φ=12 mm) cells were assembled using glass fiber as the separator (Φ=16mm) in CR2032 type battery shells. The thickness of the Zn anode used in this study is 100 μm, which corresponds to a capacity of about 58.8 mA h cm^{-2}. The amount of electrolyte added to each symmetric cell and half cell were fixed at 100 μl and the amount of electrolyte added to each full cell was fixed at 300 μl.

Electrochemical test

CV (1 mV s^{-1}; -0.3 V-0.8 V), CA and CP tests were conducted on Zn||Cu cells employing an electrochemical workstation (CHI660E). In Tafel tests, Zn foils were employed as both working electrode and counter electrode and the scan rate was 1 mV s^{-1}, the reference electrode used was Ag/AgCl. LSV was tested from -0.95 V to -1.45 V at 1 mV s^{-1}, with Zn foil as working electrode and platinum (Pt) plate as counter electrode, the reference electrode used was Ag/AgCl. CV (1 mV s^{-1}; 0.2 V-1.6 V) test of Zn|| V_2O_5 full cells employed an electrochemical workstation (CHI660E). The galvanostatic discharge-charge tests were performed on a LAND battery test system, all full cells were initially activated at a current density of 0.1 A g^{-1} for 10 cycles. For the self-discharge test of the full battery, it was first activated at 0.1 A g^{-1} for 10 cycles, followed by 10 cycles at 1 A g^{-1}, and then allowed to stand for 24 h for the self-discharge test. The Electrochemical Impedance Spectroscopy (EIS, 0.01-10^5 Hz) of Zn||Zn symmetric cells and Zn||V_2O_5 full cells were conducted on an electrochemical workstation (CHI660E) with amplitude of 5 mV.

Density functional theory (DFT) calculations

All the density functional theory (DFT) calculations were done via the Vienna Ab initio Simulation Package (VASP).[1] The generalized gradient approximation (GGA) with the exchange-correlation functional Perdew-Burke-Ernzerhof (PBE) was used.[2] A cutoff energy of 520 eV was set for the exchange and correction. The convergence criteria with forces on atoms and energy residual were smaller than 0.05 eV/Å and 10^{-5} eV, respectively. Initially, the structure of each crystal was optimized, followed by the construction of the corresponding unit cell box. A 15Å vacuum layer was included above the crystal plane to mitigate the influence of repetitive structures on subsequent calculations. with a k-point set of 3×3×1. DFT-D3 correction was applied to address intermolecular dispersion forces.[3]

The calculation method for adsorption energy (E) is as follows:

$$E = E_{ab} - E_a - E_b$$

Here, E_{ab} represents the energy of the system after adsorption, while E_a and E_b denote the energies of the two components before adsorption, respectively. The electrostatic potential (ESP) analyses are based on the Materials Studio. ΔG_{H*} was calculated as:

$$\Delta G_{H*} = \Delta E_{DFT} + \Delta E_{ZPE} - T\Delta S$$

where ΔE_{DFT}, ΔE_{ZPE}, and $T\Delta S$ denote DFT calculated E_{ads}, change of zero-point energy, and change of entropic contribution, respectively.[4]

Molecular dynamics (MD) simulation

All MD simulation for solvation structure investigation was conducted with the Forcite module with the COMPASS III force field. We constructed the simulated solution box and made this box energy minimum. The box dimensions were set at 28.66 Å × 28.66 Å × 28.66 Å, employing periodic boundary conditions in all three axes. Each simulation cell consisted of 510 H_2O molecules, 50 $ZnSO_4$ molecules, and 15 BED. After equilibrium in the NPT ensemble 1 ps, the box with a size of 25.43 Å × 25.43 Å × 25.43 Å. Following that, the solution models were equilibrated for a 400 ps system duration

under constant pressure and temperature conditions. The time step was set as 1.0 fs. Finally, radial distribution function (RDF) was analysis on the final trajectory to examine intermolecular interactions between different atoms.

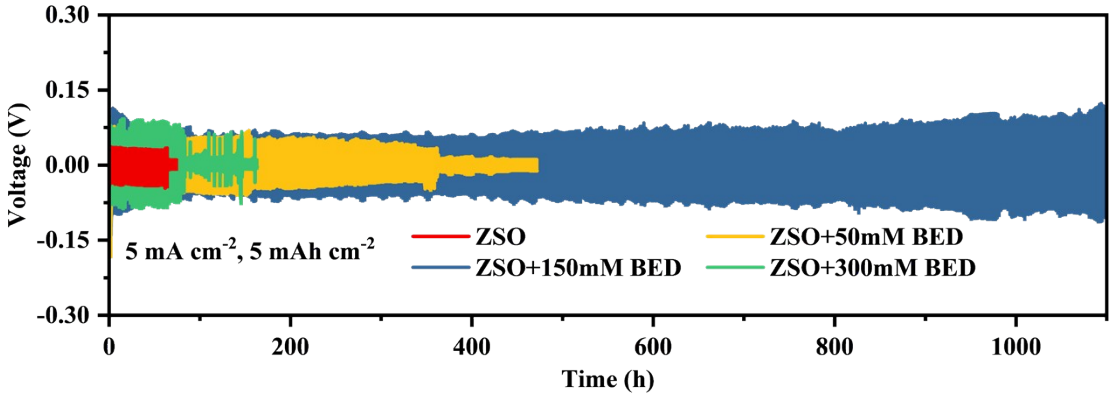

Figure S1. Zinc plating/stripping profile of Zn||Zn symmetric cells in different concentration of BED electrolytes at 5 mA cm^{-2} and 5 mAh cm^{-2}.

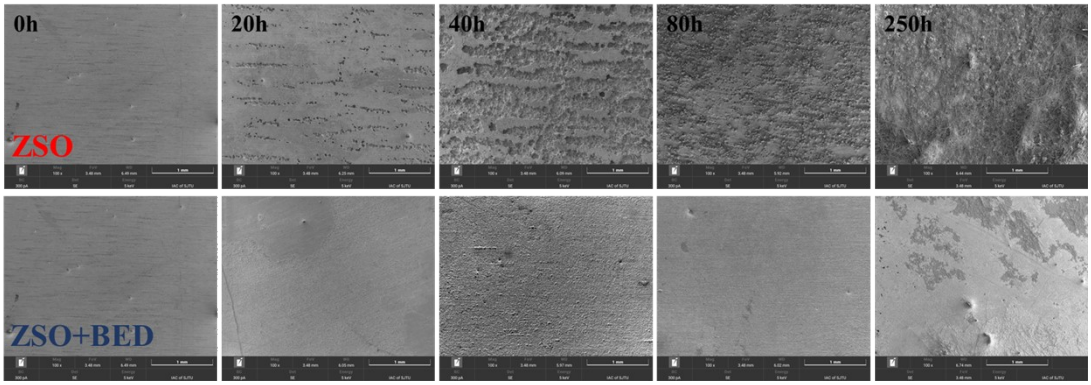

Figure S2. The SEM at 100× magnification of zinc electrode cycled 0h, 20h, 40h, 80h and 250h in different electrolytes at 1 mA cm^{-2} and 1 mA h cm^{-2} .

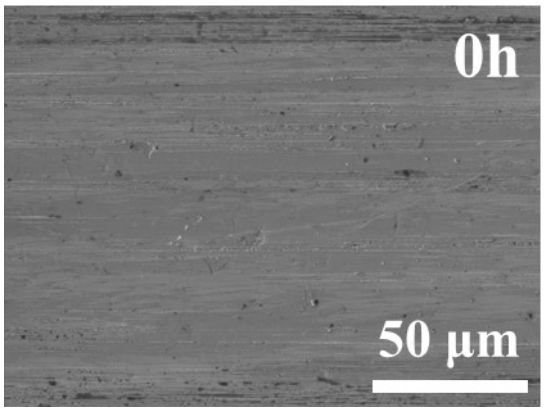

Figure S3. The SEM of primitive zinc electrode at 2000× magnification.

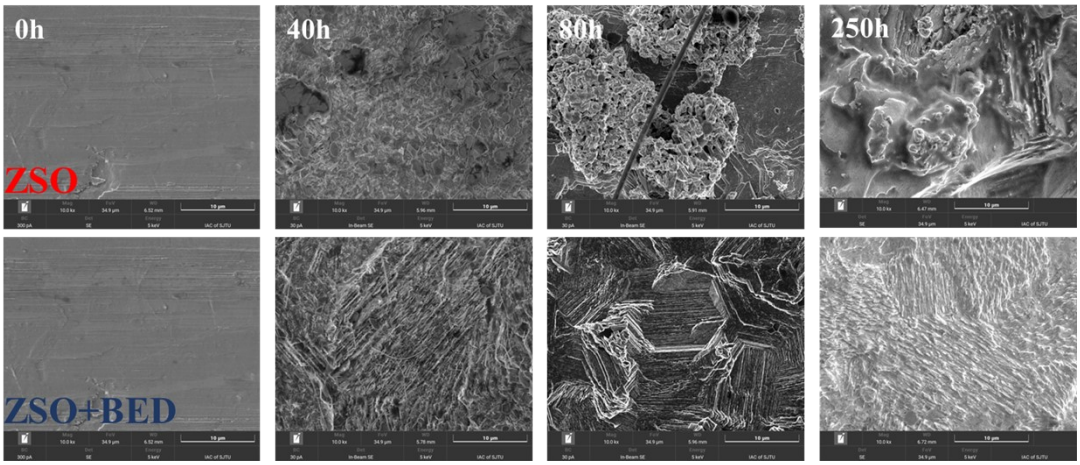

Figure S4. The SEM at 10000× magnification of zinc electrode cycled 0h, 40h, 80h and 250h in different electrolytes at 1 mA cm^{-2} and 1 mA h cm^{-2}.

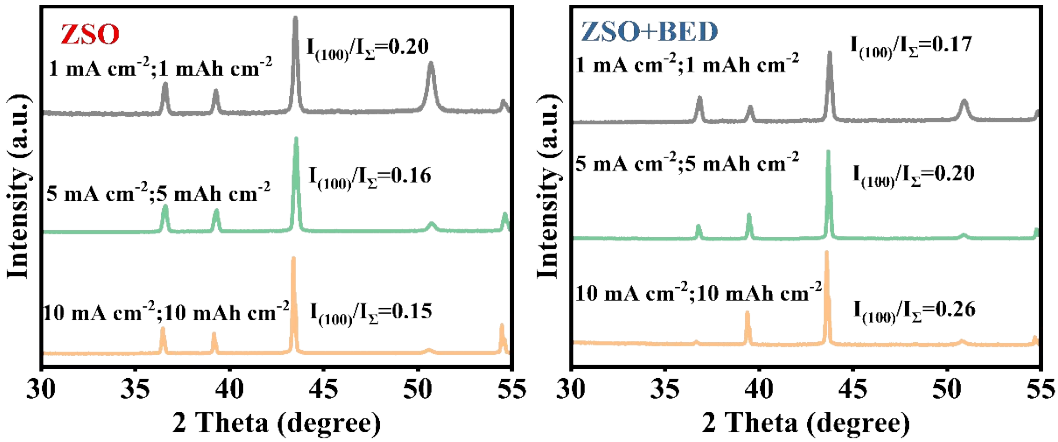

Figure S5. XRD patterns of zinc deposits on Cu at different current densities and areal capacities. ($I_{\Sigma}=I_{(002)}+I_{(100)}+I_{(101)}$)

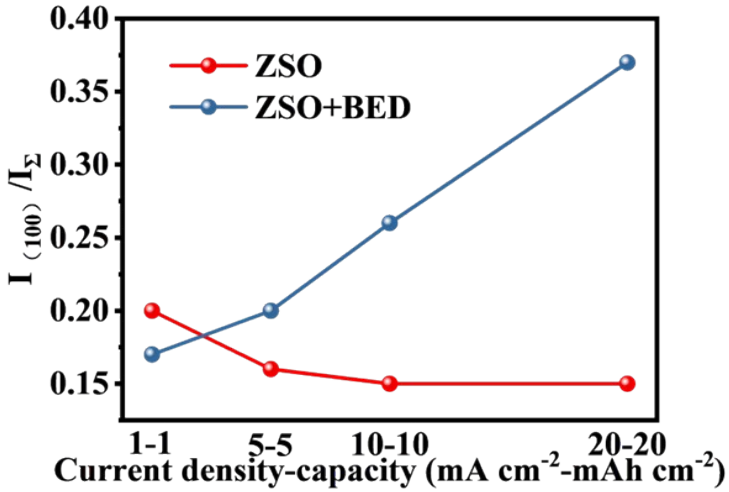

Figure S6. Relative intensity changes of Zn(100) peak under different deposition conditions. ($I_{\Sigma}=I_{(002)}+I_{(100)}+I_{(101)}$)

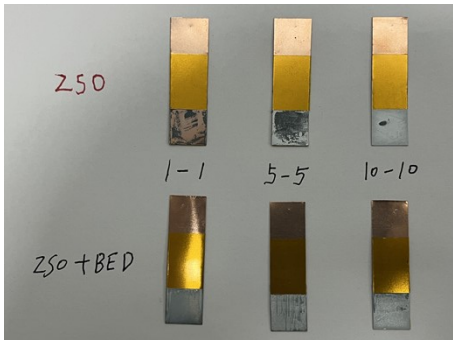

Figure S7. Optical photographs of zinc electrodeposited under various current densities and surface capacities.

The zinc deposited in ZSO formed a moss-like structure that does not uniformly cover the copper substrate at 1 mA cm^{-2} -1 mA h cm^{-2} (Figure S7). Thus, its XRD results were less reliable in reflecting its true deposition orientation at this condition.

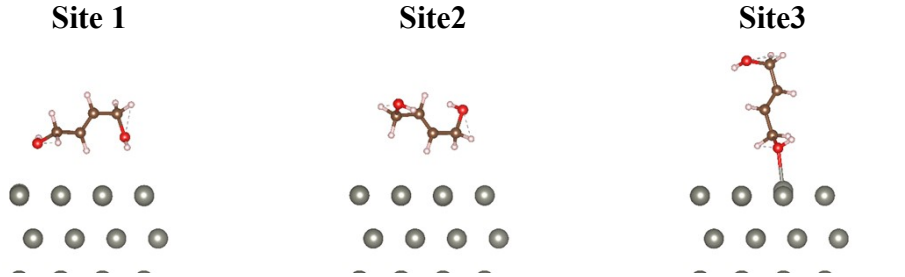

Figure S8. Adsorption energy of BED at different sites on zinc (002).

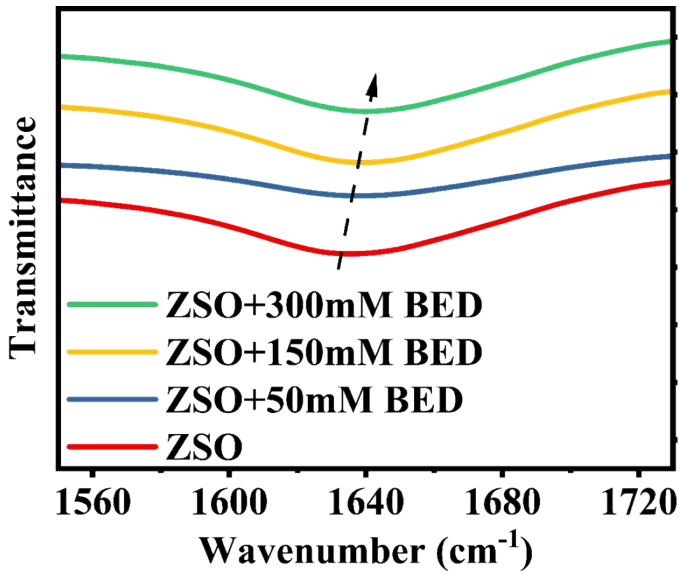

Figure S9. FTIR spectra of different electrolytes in the wavelength range of 1560 cm^{-1} -1720 cm^{-1}.

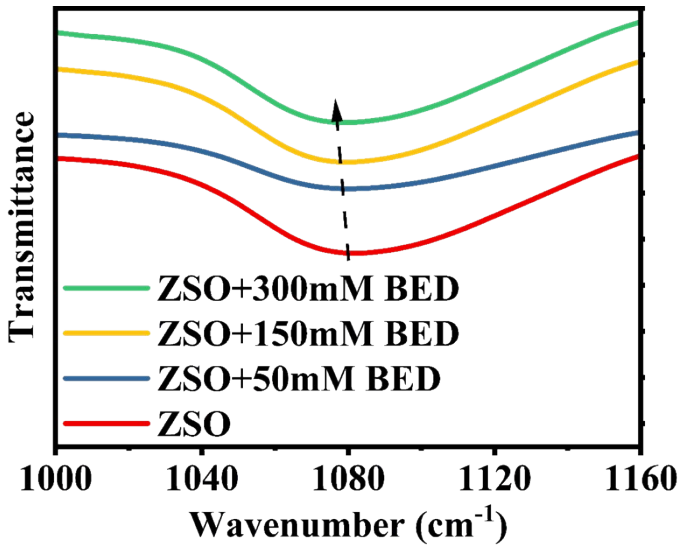

Figure S10. FTIR spectra of different electrolytes in the wavelength range of 1000 cm^{-1} -1160 cm^{-1}.

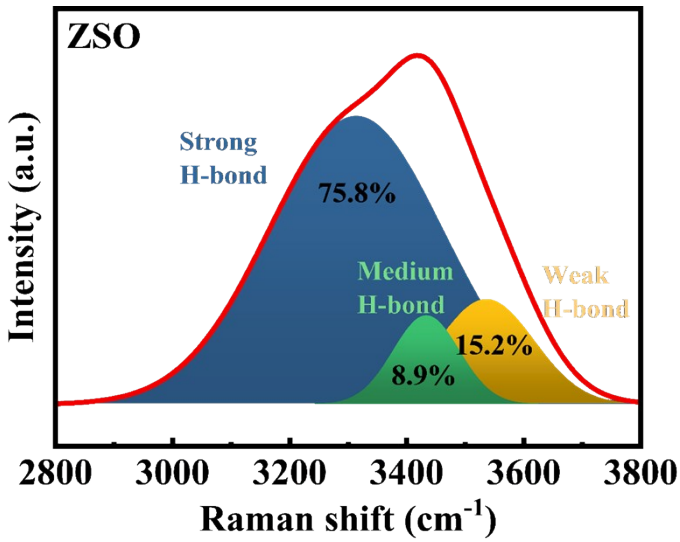

Figure S11. Raman spectra of O-H bond in ZSO electrolytes.

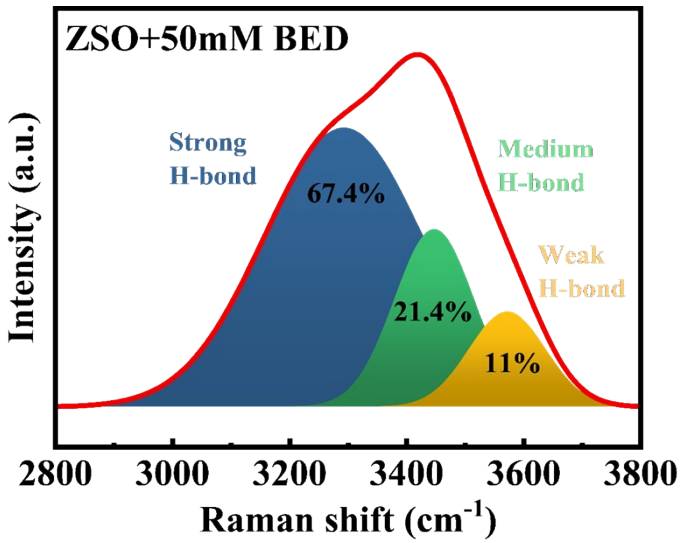

Figure S12. Raman spectra of O-H bond in ZSO+50mM BED electrolytes.

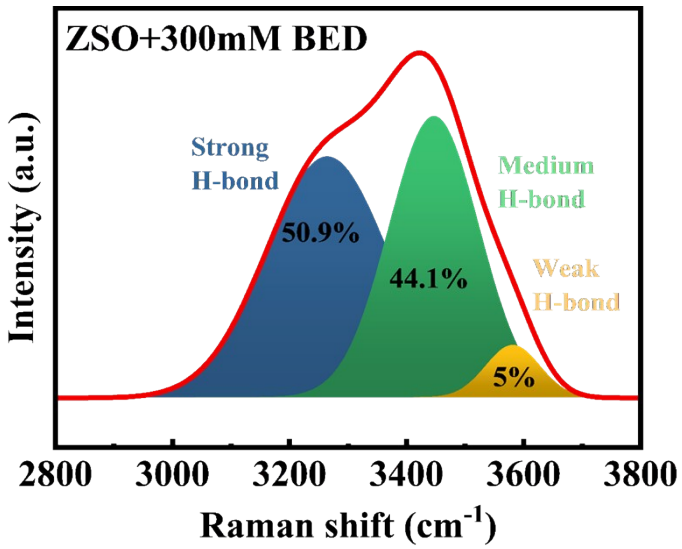

Figure S13. Raman spectra of O-H bond in ZSO+300mM BED electrolytes.

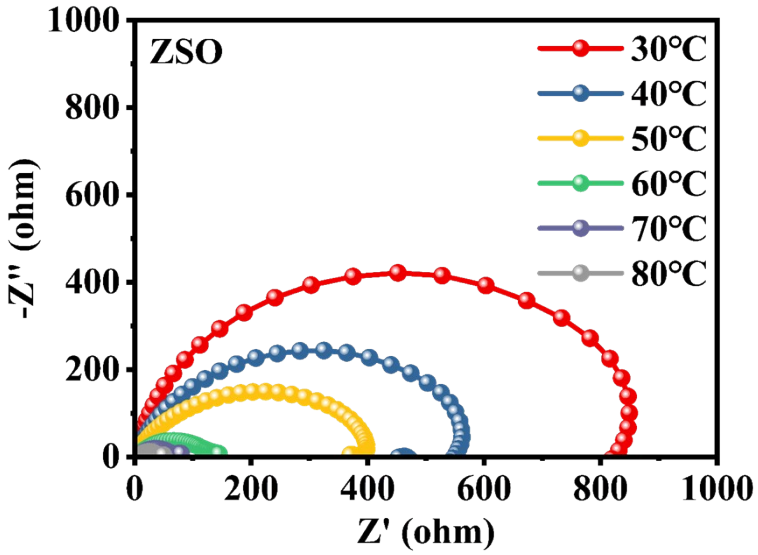

Figure S14. EIS of Zn||Zn symmetric cells using ZSO electrolyte in the range of 30°C-80°C.

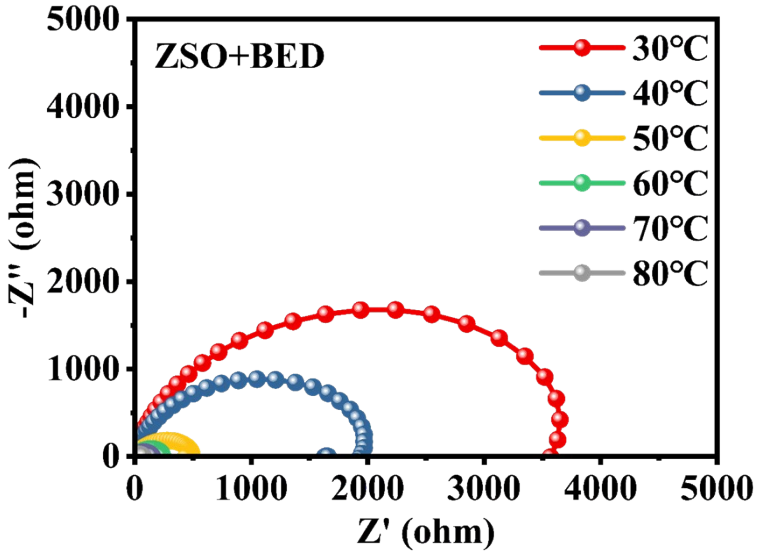

Figure S15. EIS of Zn||Zn symmetric cells using ZSO+BED electrolyte in the range of 30°C-80°C.

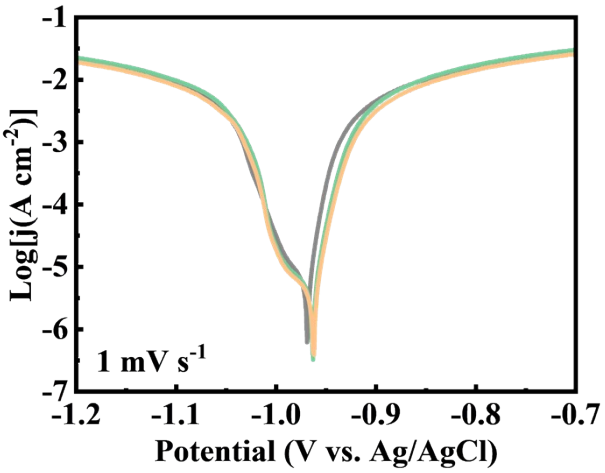

Figure S16. Three Tafel Tests of zinc in ZSO+BED Electrolyte.

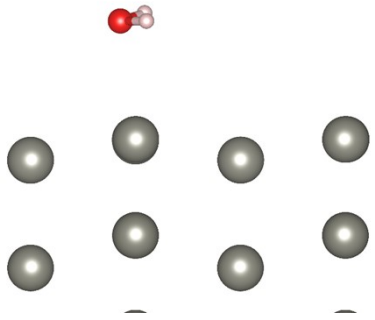

Figure S17. Adsorption energy of H_2O on Zn(100)

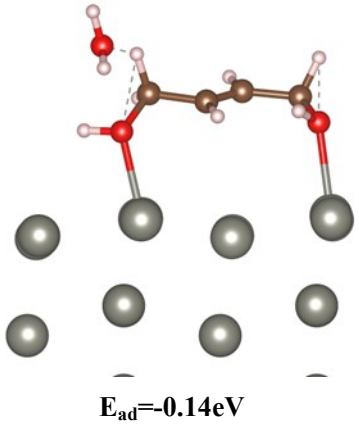

Figure S18. Adsorption energy of H_2O on Zn(100) with BED

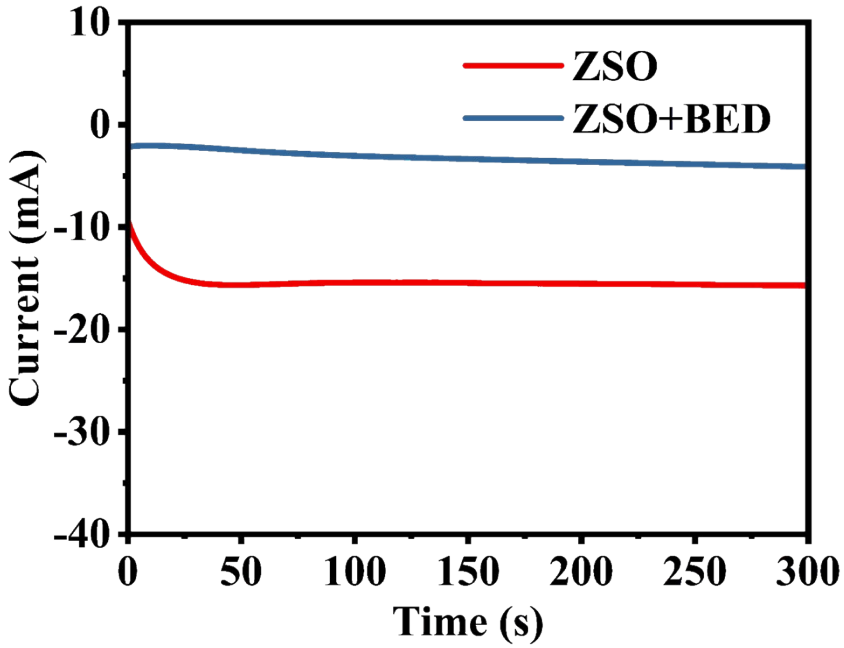

Figure S19. Chronoamperometry curves of Zn||Cu half cells with different electrolytes.

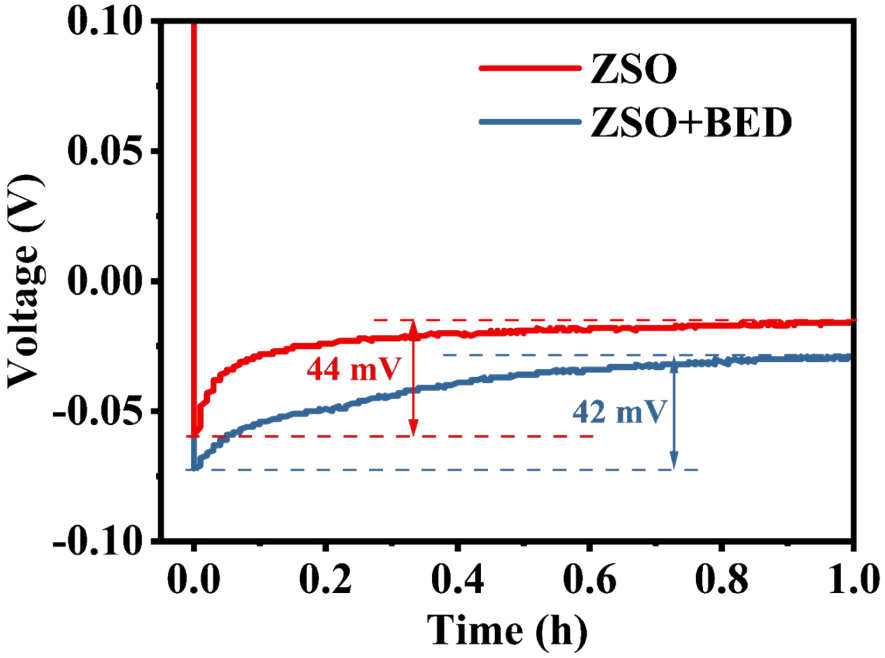

Figure S20. Chronopotentiometry curves of Zn||Cu half cells with different electrolytes.

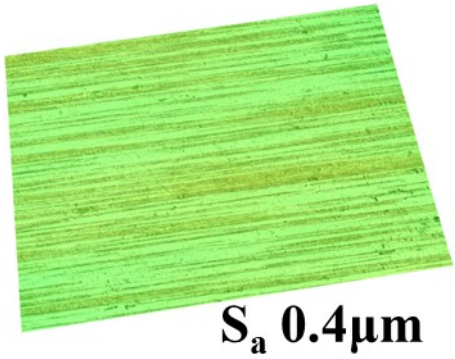

Figure S21. The CLSM of primitive zinc electrode at 25× magnification.

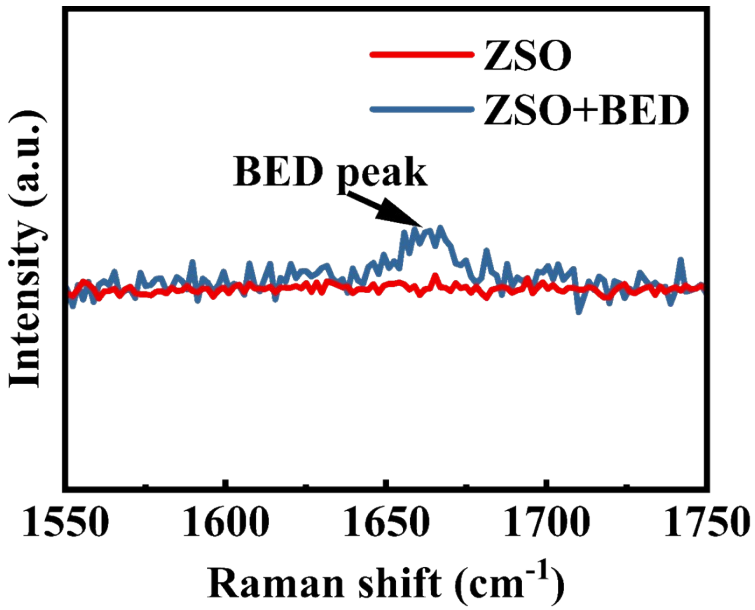

Figure S22. Raman characteristic peaks appearing after adding BED to ZSO.

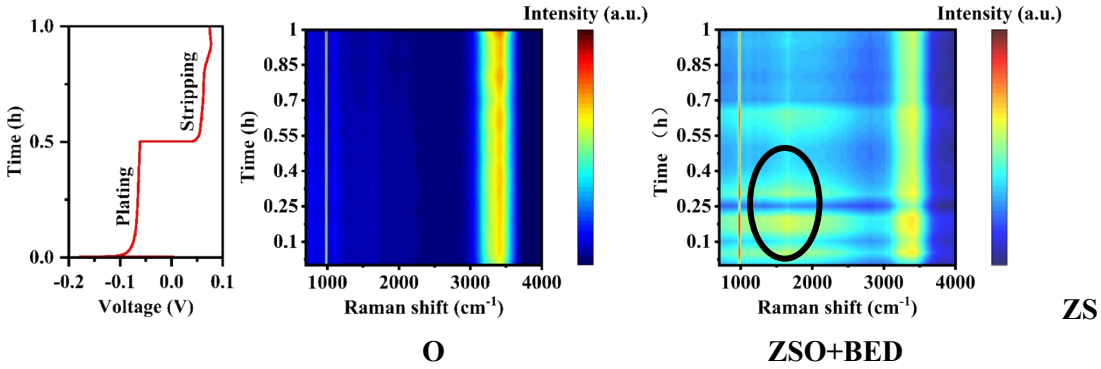

Figure S23. 2D In situ Raman spectroscopy of the anode during electroplating and stripping in Zn||Zn symmetric cells in different electrolytes.

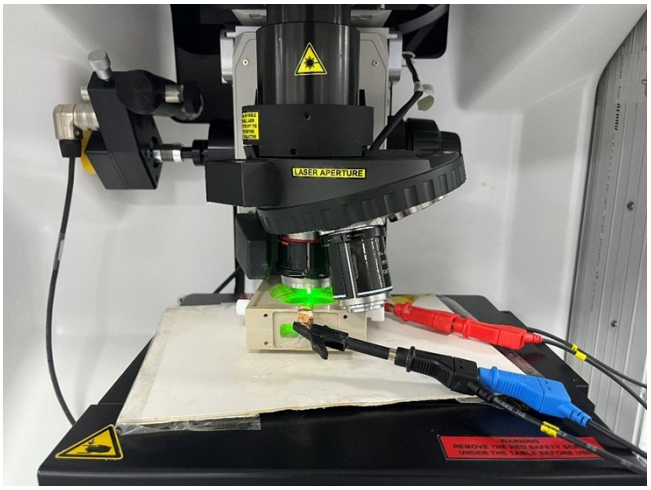

Figure S24. Optical photograph of the instrument used to perform in-situ Raman testing

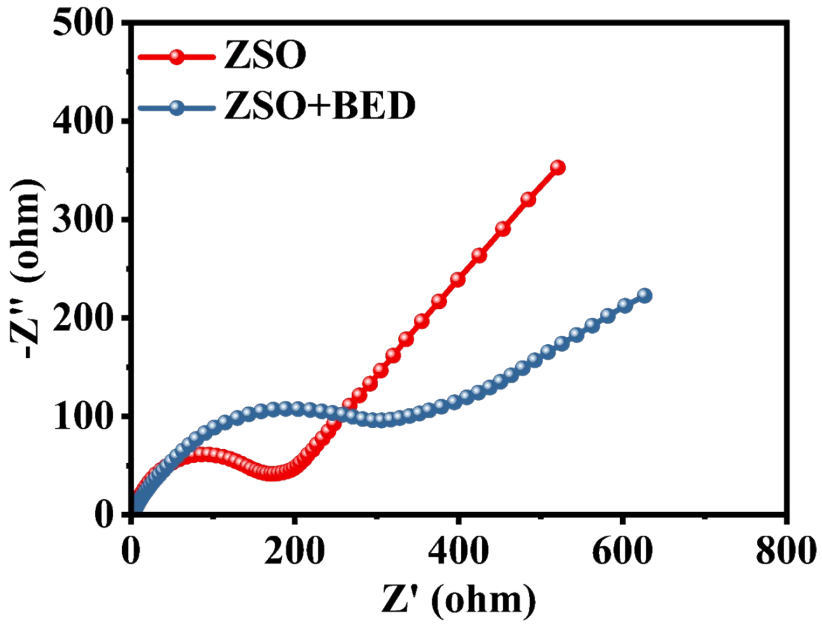

Figure S25. EIS of fresh full cells using different electrolytes.

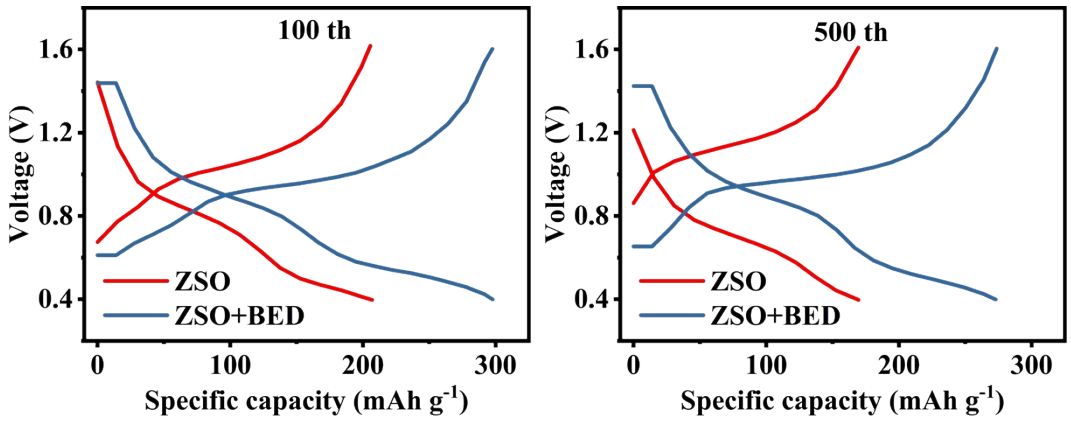

Figure S26. Different cycles of charge/discharge profiles of Zn||V_2O_5 full cells at 5 A g^{-1} in different electrolytes.

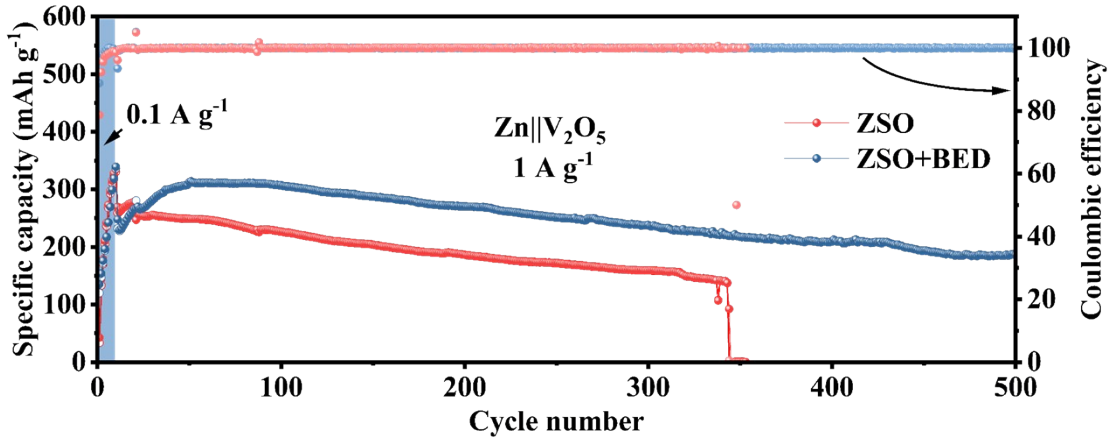

Figure S27. Long-term cycling performance of Zn||V_2O_5 full cells at 1 A g^{-1} in different electrolytes

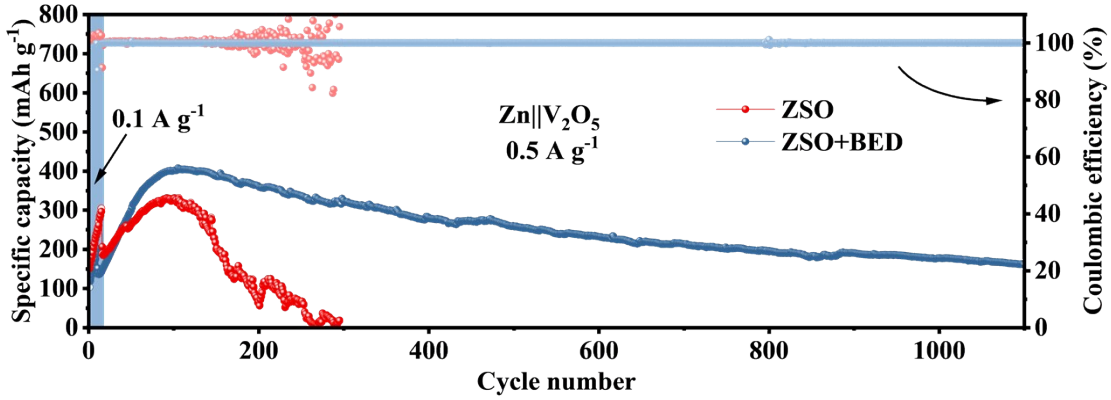

Figure S28. Long-term cycling performance of Zn||V_2O_5 full cells at 0.5 A g^{-1} with different electrolytes

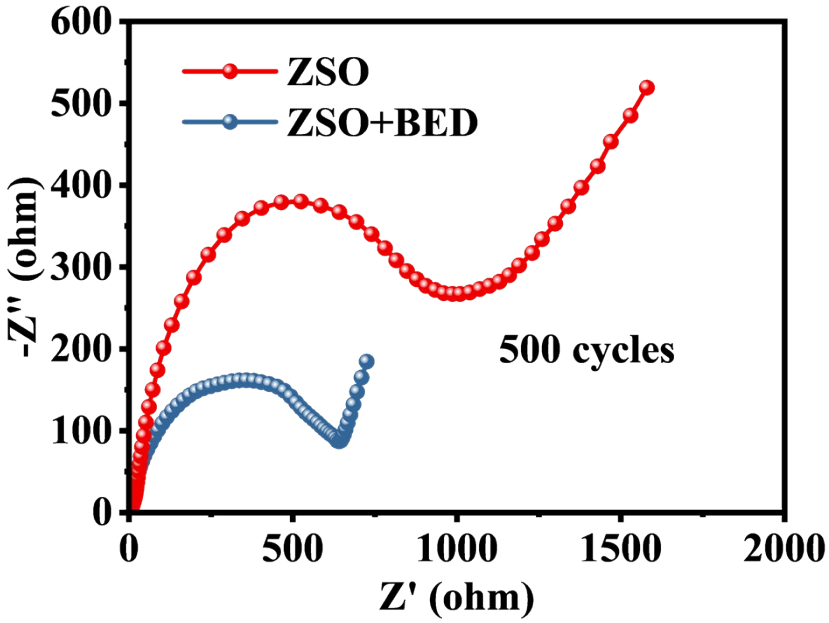

Figure S29. EIS of full cells after 500 cycles at 1 A g^{-1} in different electrolytes.

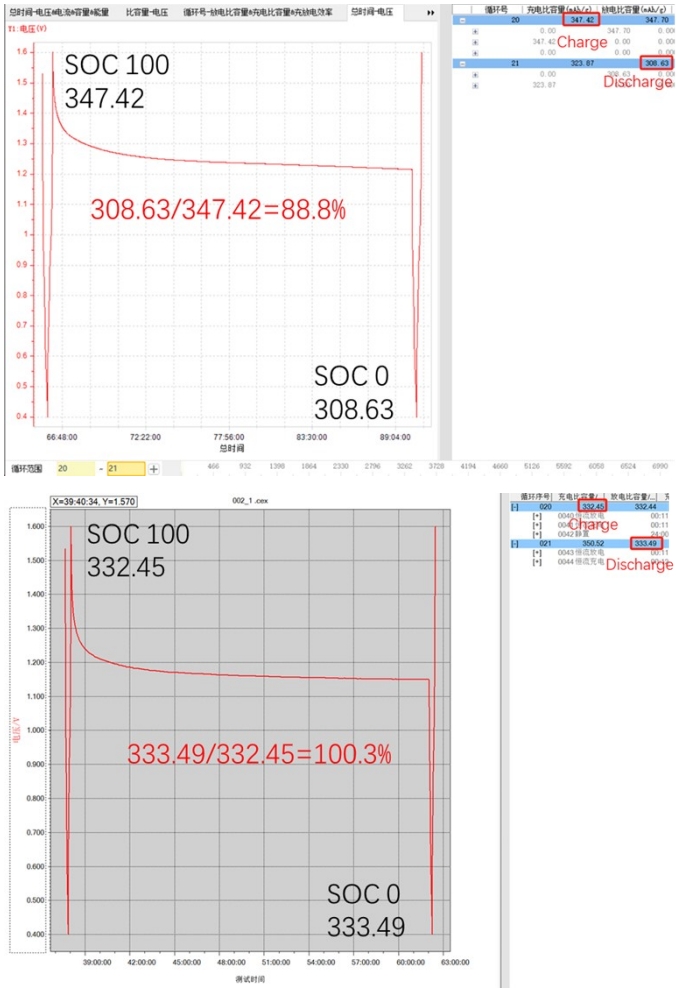

Figure S30. Raw date of self–discharge test of Zn||V_2O_5 full cells.

Table S1. Comparison with DOD performance in recent reports

Electrolytes	Additives	DOD	Cycle time	Reference s
2M $ZnSO_4$	2-butene-1,4-diol	67.7%	350h	This work
2M $ZnSO_4$	2-methylimidazole	34%	400h	5
2M $ZnSO_4$	Zinc acetylacetonate	68.5%	250h	6
2M $ZnSO_4$	YCl_3	68.3%	130h	7
2M $ZnSO_4$	Sucral	42.5%	200h	8
2M $ZnSO_4$	C_8TAB	20%	300h	9
2M $Zn(OTF)_2$	N,N-dimethyl-1Himidazole-1-sulfonamide	50%	380h	10
2M $ZnSO_4$	Lactobionic acid	92%	60h	11
2M $ZnSO_4$	cucurbit[6]uril	34.2%	450h	12
3M $ZnSO_4$	2,2′,2″-nitrilotriethanol	70%	220h	13

Table S2. Comparison with full cells performance in recent reports

Full cells	Current density ($A\ g^{-1}$)	Cycle number	Final capacity ($mA\ h\ g^{-1}$)	Reference s
Zn| ZSO+BED $\|V_2O_5$	0.5	1100	177.9	This work
	5	1000	218.1	

Zn| ZSO+C_5SeCN |V_2O_5	2	450	100	14
Zn| $Zn(OTF)_2$ | NH^{4+}-V_2O_5	1	1000	182.1	15
Zn| ZSO+ β-CD |MnO_2	5	1000	80	16
Zn| $Zn(OTF)_2$ | BM |NVO	10	1000	110	17
Zn| ZSO+EDTA |VO_2	4	2000	120	18
Zn| $Zn(OTF)_2$+IS4 |NVO	1	1200	250.2	19
Zn| ZSO+CTAB |ZVO	1	500	230	9
	5	1000	260	
SAM-Zn| ZSO |NVO	5	1000	200	20
Zn| ZSO+C4 |ZVO	5	1000	150	21
ZnO(002)| ZSO |V_2O_5	1	1000	113	22
Zn| ZSO+Mlz |MnO_2	1	800	80	5

References

1. G. Kresse and J. Furthmüller, *Computational materials science*, 1996, **6**, 15-50.
2. J. P. Perdew, K. Burke and M. Ernzerhof, *Physical review letters*, 1996, **77**, 3865.
3. S. Grimme, J. Antony, S. Ehrlich and H. Krieg, *The Journal of chemical physics*, 2010, **132**.
4. R. Zhao, X. Dong, P. Liang, H. Li, T. Zhang, W. Zhou, B. Wang, Z. Yang, X. Wang and L. Wang, *Advanced Materials*, 2023, **35**, 2209288.
5. J. Cao, M. Sun, D. Zhang, Y. Zhang, C. Yang, D. Luo, X. Yang, X. Zhang, J. Qin and B. Huang, *ACS nano*, 2024.
6. X. Xiao, X. Ye, Z. Wu, X. Wu, J. Yu, L. Gu and S. Liu, *Advanced Materials*, 2024, **36**, 2408706.
7. Y. Chen, S. Zhou, J. Li, J. Kang, S. Lin, C. Han, H. Duan, S. Liang and A. Pan, *Advanced Energy Materials*, 2024, 2400398.
8. Q. Zhao, W. Liu, X. Ni, H. Yu, C. Zhang, B. Wang, L. Jiang, H. He, Y. Chen and L. J. A. F. M. Chen, *Advanced Functional Materials*, 2024, DOI: 10.1002/adfm.202404219, 2404219.
9. D. Tang, X. Zhang, D. Han, C. Cui, Z. Han, L. Wang, Z. Li, B. Zhang, Y. Liu and Z. Weng,

Advanced Materials, 2024, **36**, 2406071.

10. L. Liu, X. Wang, Z. Hu, X. Wang, Q. Zheng, C. Han, J. Xu, X. Xu, H. K. Liu and S. X. J. A. C. Dou, *Angewandte Chemie-International Edition*, 2024, DOI: 10.1002/anie.202405209, e202405209.
11. M. Shi, C. Lei, H. Wang, P. Jiang, C. Xu, W. Yang, X. He and X. J. A. C. I. E. Liang, *Angewandte Chemie-International Edition*, 2024, DOI: ARTN e20240726110.1002/anie.202407261, e202407261.
12. X. Yang, Y. Zhao, S. Lv, L. Zhong, C. Yue, S. Zhan, L. Zhao, C. Wang, X. Li and X. Liu, *Energy & Environmental Science*, 2024.
13. K. Wang, T. Qiu, L. Lin, H. Zhan, X.-X. Liu and X. Sun, *Energy Storage Materials*, 2024, 103516.
14. R. Han, T. Jiang, Z. Wang, R. Xue, X. Liu, Y. Tang, Z. Qi and Y. Ma, *Advanced Functional Materials*, 2024, 2412255.
15. J. Feng, X. Li, Y. Ouyang, H. Zhao, N. Li, K. Xi, J. Liang and S. Ding, *Angewandte Chemie*, 2024, e202407194.
16. G. Zhang, L. Fu, Y. Chen, K. Fan, C. Zhang, H. Dai, L. Guan, M. Mao, J. Ma and C. Wang, *Advanced Materials*, 2024, **36**, 2405949.
17. J. Ma, X. Shi, Z. Wang, L. Zhou, X. Liu, X. Lu and Z. Jiang, *Advanced Materials*, 2024, 2406429.
18. S. J. Zhang, J. Hao, D. Luo, P. F. Zhang, B. Zhang, K. Davey, Z. Lin and S. Z. Qiao, *Advanced Energy Materials*, 2021, **11**, 2102010.
19. L. Liu, X. Wang, Z. Hu, X. Wang, Q. Zheng, C. Han, J. Xu, X. Xu, H. K. Liu and S. X. Dou, *Angewandte Chemie*, 2024, **136**, e202405209.
20. D. Li, Y. Tang, S. Liang, B. Lu, G. Chen and J. Zhou, *Energy & Environmental Science*, 2023, **16**, 3381-3390.
21. Z. Hu, F. Zhang, F. Wu, H. Wang, A. Zhou, Y. Chen, T. Xue, R. Chen and L. Li, *Energy & Environmental Science*, 2024.
22. C. Yang, P. Woottapanit, S. Geng, K. Lolupiman, X. Zhang, Z. Zeng, G. He and J. Qin, *Advanced Materials*, 2024, 2408908.